PAPER

Check for updates

Design, preparation and characterization of magnetic nanoparticles functionalized with chitosan/Schiff base and their use as a reusable nanocatalyst for the green synthesis of 1*H*-isochromenes under mild conditions†

Mahshid Zarei and Hossein Naeimi [ID] *

In this study, a Schiff base complex magnetic nanocatalyst was designed and prepared. The structure of the $Fe_3O_4@CS-SB-CaMgFe_2O_4$ nanocatalyst was characterized using FT-IR spectroscopy, XRD, VSM, FE-SEM, EDX, elemental mapping, BET, and TGA techniques. The synthesis of 1*H*-isochromene compounds has attracted the attention of chemists due to their biological and medicinal properties. The 1*H*-isochromene derivatives were synthesized in the presence of the $Fe_3O_4@CS-SB-CaMgFe_2O_4$ nanocatalyst with excellent efficiency and short reaction time as well as according to the rules of green chemistry. This reaction was carried out using $Fe_3O_4@CS-SB-CaMgFe_2O_4$ as a catalyst to develop a simple method with low activation energy at room temperature under optimal conditions. This catalyst provides a promising route for the synthesis of 1*H*-isochromene multiple times through its recyclability without significant loss of catalytic activity. This nanocatalyst possesses several advantages, including cost-effectiveness, facile separation, environmental friendliness, and recyclability, for the efficient production of 1*H*-isochromenes. The obtained compounds were further analyzed using spectroscopic techniques, such as melting point, FT-IR, ^1H NMR, and ^{13}C NMR analyses, to confirm their structures. The spectra of the synthesized compounds were recorded and analyzed, and a plausible mechanism for their synthesis was proposed. The characterization results and structural elucidation provide valuable insights into the preparation of these compounds.

1. Introduction

Schiff bases are compounds with a crystalline structure and weak basic properties[1] and are easily synthesized from condensation between primary amines and compounds with carbonyl groups such as aldehydes and ketones.[2] Schiff bases are named after Nobel Prize-winning German chemist Hugo Schiff, who discovered this compound in 1864.[3]

Azomethine nitrogen coordinates metal ions *via* the formed Schiff bases from amines and carboxylic acids.[4] These compounds are very important and widely used because of their interesting physical and chemical properties.[5] A range of biological effects have also been reported for Schiff bases, including antifungal, antipyretic,[6] antibacterial,[7] antimalarial, and antiproliferative[8] effects. These compounds are excitingly used as pigments and dyes, catalysts, and polymer stabilizers.[9]

Department of Organic Chemistry, Faculty of Chemistry, University of Kashan, Kashan, 87317-51167, I.R. Iran. E-mail: naeimi@kashanu.ac.ir; Fax: +98 3155912397; Tel: +98 3155912388

Besides their structural similarity to natural biological substances, they contain an azomethine group (–N=CH–), which is a crucial factor in explaining the mechanisms that lead to racemization and transformation in biology.[10]

One of the branches of nanoscience is magnetic and metal nanoparticles; in these compositions, the number of molecules placed on the surface increases by reducing the size of the particles, which creates special properties. These combinations have become wide and diverse substrates, such as alumina, carbon, silica, and polymers, can be used to design and produce various nanocatalysts. Considering the easy preparation, low price, and chemical stability of magnetic nanoparticles, such as maghemite (γ-Fe_2O_3) and magnetite (Fe_3O_4), they can be considered suitable and ideal substrates for stabilizing catalytic materials. They can also be recovered by applying an external magnetic field.[11,12] When the size of these nanoparticles is between 10 and 20 nm, these particles will have the best performance. These nanoparticles are widely used in various fields, such as energy storage, data storage, magnetic ink for printers and bank checks, removing water pollution, absorbing pollutant particles,[13] and biomedicine.[14]

Chitosan is a modified biopolymer, derived by partial deacetylation of chitin.[15] Besides many physical and chemical properties, chitosan has significant solubility and chemical activity.[16] In addition to its biological properties like anti-tumor, antibacterial,[17] antifungal, biocompatibility,[18] degradability,[19] and low toxicity, chitosan also has chemical properties including amine and hydroxy active groups, hydrophilicity, and poly structure.[20] These properties makes it an excellent absorbent for iron nanoparticles because of its ability and affinity for macromolecules. These materials are cheap and have properties that can be used in various fields such as food, Medicine, biotechnology, and medical research.[21]

To increase the chemical stability and biocompatibility of iron oxide nanoparticles, a cover can be applied.[22] Among these polymers, chitosan is a suitable polymer for optimizing iron nanoparticles. This biopolymer, which is present in the walls of different cells of fungi, is one of the most abundant polymers in nature.[23] Superparamagnetic nanoparticles are coated with a polymer, which is typically a magnetic core. The polymer shell is then assigned to a desired functional group.[24]

Some of the most important features are the possibility of simple and fast extraction by only using an external magnetic field, no need for smoothing and centrifuging steps during the extraction process, and the ability to extract large volumes of samples, and control and transfer them using an external field.[25]

The isochromene compounds with oxygen in their ring structure are widely recognized and important. The benzopyran compound is known as isochromene when the oxygen atom is positioned in the second instead of the first position.[26] Because these compounds have many biological and medicinal properties,[27] they have attracted the attention of many chemists. Nowadays, researchers are looking at the preparation and production of these compounds and their derivatives to observe the principles of green chemistry and modern methods.[28]

In 2000, Sito et al. prepared the 1H-isochromene derivative with a favorable yield using benzaldehyde, malononitrile and cyclohexanone derivatives in the presence of a triethylamine catalyst.[29] In 2021, Thomson and co-workers synthesized 1,5,8-trimethoxy-1H-isochromene-3-carboxylate through a seven-step reaction in the presence of a palladium catalyst.[30] Also in 2021, Chen and co-workers prepared a 1-cyano isochromene compound easily with high efficiency by using 1-methoxy-1H-isochromene and trimethylsilyl cyanide in the presence of $Fe(OTf)_3$ catalyst.[31]

In continuation of the ongoing work by our team on catalytic reactions,[32,33] the purpose of this research was to create a novel catalyst with high reactivity through a simple procedure. Therefore, the magnetic nanoparticles functionalized with chitosan were fabricated and used for multi-component reaction of cyclohexanone, malononitrile and aromatic aldehyde in ethanol solution at room temperature under mild conditions. In this protocol, the 1H-isochromene derivatives were purely obtained with high efficiency and short reaction times. This research aims to improve reaction efficiency and reduce the reaction time through the usage of a chitosan-functionalized Schiff base magnetic nanocatalyst that can be reused.

2. Experimental

2.1. Chemicals

All chemicals in this research, including cyclohexanone, various derivatives of aromatic aldehydes, and malononitrile, as well as various metal salts, cetyltrimethyl ammonium bromide, guanidine, and chitosan were obtained from Merck and Sigma Aldrich Chemical Companies.

The FT-IR spectra were recorded on an FT-IR Magna 550 spectrometer using KBr plates in the 400–4000 cm^{-1} range. The ^1H NMR measurements were performed in DMSO-d_6 and $CDCl_3$ solvents using a Bruker Avance-400 MHz spectrometer with $Si(CH_3)_4$ as a chemical shift reference. Melting points were measured using Yanagimoto micro melting point equipment and are uncorrected. Homogenization was achieved using a BANDELIN ultrasonic HD 3200 probe model KE76 with a 6 mm diameter. In Iran (Kashan University), the magnetic measurement of the sample was performed using a vibrating sample magnetometer (VSM) at 300 K. A Philips X'PertPro apparatus provided XRD patterns using CuKa radiation ($\lambda = 0.154056$ angstrom wavelength) in the range of 10–80° (2θ). The specific surface area and porosity of nanocatalysts were measured using a nine-point surface area measuring device, model BELSORP-mini II, made in Japan. The structure of the catalyst was investigated using the X-ray electron scattering method with an Oxford company device. The TGA images of the magnetic nanocatalysts were recorded using an STA 504 device at Kashan University. An FE-SEM (model MIRA3) with a 15 kV accelerating voltage was used to analyze the morphology of the nanoparticles.

2.2. Preparation of Fe_3O_4 magnetic nanoparticles functionalized with chitosan

Fe_3O_4@CS NPs were made using chemical co-precipitation.[24] First, 1.5 g of chitosan was dissolved in 40 mL of acetic acid solution (0.5 M). Then, 0.25 mmol of $FeCl_3 \cdot 4H_2O$ and 0.5 mmol of $FeCl_2 \cdot 6H_2O$ (with a molar ratio of 2 : 1) were added to the mixture and it was stirred for 6 hours under N_2 gas at 80 °C. Then, a 25% by-weight solution of ammonium hydroxide (NH_4OH) was added drop by drop to the reaction mixture until the pH of the solution reached 11. The mixture was again exposed to nitrogen gas and subjected to reflux conditions for 30 minutes at 80 °C. The contents of the balloon were separated using a centrifuge and washed several times to neutralize the pH of the solution. The resulting sediment was dried for 24 hours in an oven at 70 °C.

2.3. Preparation of Fe_3O_4@CS NPs functionalized with a Schiff base

1.0 g of Fe_3O_4 functionalized with chitosan and 0.5 g of terephthalaldehyde were poured into a round-bottom flask with two openings, and the resulting mixture was placed in 40 mL of ethanol under nitrogen gas for 30 h under reflux conditions. After completion of the reaction, the mixture was cooled to room temperature. Then, the contents of the flask were separated through centrifugation and washed multiple times. Finally, the obtained sediment was dried at room temperature for 12 hours.

2.4. A procedure for preparation of CaMgFe₂O₄ magnetic nanoparticles

In a round bottom flask, 1 mmol of calcium chloride (0.11 g), 1 mmol of magnesium chloride (0.09 g), and 4 mmol of iron(III) chloride (0.64 g) were poured and dissolved in 40 mL of distilled water. Then, 1 mmol (0.19 g) of citric acid was added as a surfactant and the reaction mixture was kept under reflux conditions for 7 hours. Ammonium hydroxide (NH₄OH) was then slowly added to the reaction mixture until the pH of the solution reached 7. The reaction mixture was then refluxed again for 5 hours. After the completion of the reaction, the mixture was separated using a centrifuge and washed with water and ethanol, and the obtained sediment was dried in an oven at 70 °C for 24 hours. The resulting sediment was calcined at 300 °C for 3 hours.

2.5. Preparation of a Schiff base complex of Fe₃O₄@CS-SB-CaMgFe₂O₄ magnetic nanoparticles

In a 100 mL two-mouth flask, 0.5 g of Fe₃O₄@CS-Schiff base and 0.5 g of CaMgFe₂O₄ were added and the resulting mixture was kept in 30 mL of ethanol at a temperature of 50 °C for 20 h and refluxed under nitrogen gas. After the completion of the reaction, the black precipitate was separated using a centrifuge and washed three times with deionized water and ethanol. The obtained sediment was dried for 24 h at 40 °C (Fig. 1).

2.6. General procedure for the multicomponent synthesis of 1*H*-isochromenes

The 1*H*-isochromene was synthesized through the MCR. In this reaction, 1 mmol of cyclohexanone and 1 mmol of malononitrile were mixed in 5 mL ethanol as the solvent. After adding 10 mg of Fe₃O₄@CS-SB-CaMgFe₂O₄, the mixture was stirred at 25 °C for 5–10 minutes. 1 mmol of benzaldehyde was added after the first step was completed, and the reaction was allowed to proceed at room temperature for 10–15 minutes. After the completion of the reaction, the nanocatalyst was separated from the reaction mixture using an external magnet. Then, the reaction mixture was filtered using a porous glass filter with the help of a vacuum pump. At the end of reaction, to purify the product, the obtained precipitate was washed with *n*-hexane and distilled water and finally dried in an oven at a temperature of 80 °C for 24 hours. The obtained product was characterized by melting point, FT-IR, and ¹H NMR analyses.

3-Amino-1-(2,4-dichlorophenyl)-5,6,7,8-tetrahydro-1*H*-isochromene-4-carbonitrile (4a). White solid; mp: 275–279 °C (Lit. mp 276–279 °C);[34] IR (KBr) $\bar{\nu}$ (cm⁻¹) 3446, 3357, 3220, 2924, 2214, 1623, 1474, 1389, 1267, 1106, 1050, 876, 670; ¹H NMR (400 MHz, CDCl₃) δ (ppm) 7.59–7.63 (m, 2H), 7.44 (d, J = 8.0 Hz, 1H), 6.1 (s, 1H), 4.89 (s, 2H, NH₂), 3.99–4.01 (m, 1H), 2.80–2.82 (m, 1H), 2.20–2.35 (m, 2H), 1.80–1.82 (m, 1H), 1.56–1.58 (m, 2H), 0.95–1.05 (m, 1H).

3-Amino-1-(4-chlorophenyl)-5,6,7,8-tetrahydro-1*H*-isochromene-4-carbonitrile (4b). White solid; mp: 275–279 °C (Lit. mp 274–277 °C);[33] IR (KBr) $\bar{\nu}$ (cm⁻¹): 3418, 3341, 3243, 2939, 2211, 1643, 1601, 1492, 1392, 1273, 1095, 753, 514; ¹H NMR (400
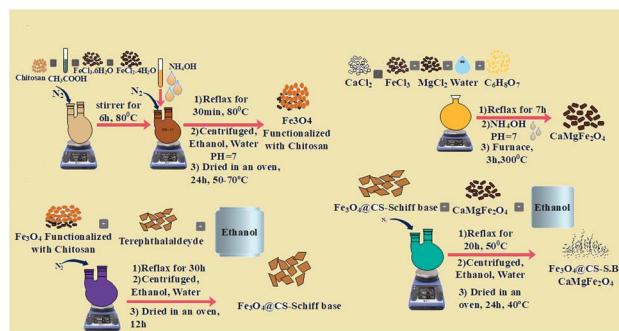

Fig. 1 The stepwise preparation of Fe₃O₄@CS-SB-CaMgFe₂O₄ magnetic nanoparticles.

MHz, CDCl₃) δ (ppm): 7.53 (d, J = 8.0 Hz, 2H), 7.44 (d, J = 8.0 Hz, 2H), 6.09 (s, 1H), 4.87 (s, 2H, NH₂), 3.08–3.11 (m, 1H), 2.83–2.86 (m, 1H), 2.30–2.35 (m, 1H), 2.17–2.21 (m, 1H), 1.81–1.84 (m, 1H), 1.67–1.70 (m, 2H), 0.93–1.03 (m, 1H).

3-Amino-1-(2-chlorophenyl)-5,6,7,8-tetrahydro-1*H*-isochromene-4-carbonitrile (4c). White solid; mp: 296–299 °C; IR (KBr) $\bar{\nu}$ (cm⁻¹): 3445, 3355, 2947, 2215, 1623, 1601, 1441, 1390, 1271, 1041, 748, 509; ¹H NMR (400 MHz, DMSO-d₆) δ (ppm): 7.78 (d, J = 8.0 Hz, 1H), 7.63 (d, J = 8.0 Hz, 1H), 7.49–7.56 (m, 2H), 7.45 (s, 2H, NH₂), 5.77 (s, 1H), 3.88–3.91 (m, 1H), 2.84–2.90 (m, 1H), 2.09–2.22 (m, 2H), 1.66–1.69 (m, 1H), 1.36–1.50 (m, 2H), 0.77–0.87 (m, 1H); ¹³C NMR (100 MHz, DMSO-d₆) δ (ppm): 143.92, 135.57, 132.27, 131.13, 130.64, 129.69, 128.86, 128.37, 121.34, 116.45, 81.92, 46.93, 34.95, 27.20, 25.21, 21.26.

3-Amino-1-phenyl-5,6,7,8-tetrahydro-1*H*-isochromene-4-carbonitrile (4d). White solid; mp: 256–260 °C (Lit. mp 255–258 °C);[32] IR (KBr) $\bar{\nu}$ (cm⁻¹): 3418, 3340, 3246, 2932, 2210, 1647, 1602, 1453, 1393, 1275, 1099, 714, 581; ¹H NMR (400 MHz, CDCl₃) δ (ppm): 7.43–7.60 (m, 5H), 6.07 (s, 1H), 4.92 (s, 2H, NH₂), 3.09–3.12 (m, 1H), 2.87–2.94 (m, 1H), 2.28–2.35 (m, 1H), 2.13–2.20 (m, 1H), 1.80–1.86 (m, 1H), 1.69–1.74 (m, 1H), 1.49–1.59 (m, 1H), 0.93–1.03 (m, 1H).

3-Amino-1-(4-bromophenyl)-5,6,7,8-tetrahydro-1*H*-isochromene-4-carbonitrile (4e). White solid; mp: 260–264 °C (Lit. mp 260–263 °C);[34] IR (KBr) $\bar{\nu}$ (cm⁻¹): 3421, 3342, 3240, 2933, 2210, 1643, 1600, 1489, 1394, 1274, 1076, 833, 510; ¹H NMR (400 MHz, DMSO-d₆) δ (ppm): 7.69 (dd, J = 8.0 Hz, 2H), 7.56 (d, J = 8.0 Hz, 1H), 7.40 (s, 1H, Ar–H, 2H, NH₂), 5.74 (s, 1H), 3.62–3.64 (m, 1H), 2.77–2.83 (m, 1H), 2.03–2.21 (m, 2H), 1.67–1.70 (m, 1H), 1.44–1.47 (m, 2H), 0.81–0.90 (m, 1H).

3-Amino-1-(4-nitrophenyl)-5,6,7,8-tetrahydro-1*H*-isochromene-4-carbonitrile (4f). White solid; mp: 230–234 °C (Lit. mp 229–232 °C);[33] IR (KBr) $\bar{\nu}$ (cm⁻¹): 3418, 3347, 3286, 2938, 2206, 1644, 1523, 1448, 1348, 1132, 1041, 859, 558; ¹H NMR (400 MHz, DMSO-d₆) δ (ppm): 8.28–8.54 (m, 1H), 8.18–8.22 (t, J = 8.0 Hz, 1H), 7.70–8.05 (m, 1H), 7.35–7.69 (m, 1H), 6.67 (s, 2H, NH₂), 5.67 (s, 1H), 3.48–3.51 (m, 1H), 3.34–3.42 (m, 1H), 2.83–2.87 (m, 1H), 2.16–2.20 (m, 1H), 2.05–2.09 (m, 1H), 1.65–1.69 (m, 1H), 1.43–1.47 (m, 1H), 0.87–0.93 (m, 1H).

3-Amino-1-(4-(dimethylamino)phenyl)-5,6,7,8-tetrahydro-1*H*-isochromene-4-carbonitrile (4g). White solid; mp: 247–250 °C (Lit. mp 248–250 °C);[32] IR (KBr) $\bar{\nu}$ (cm⁻¹): 3447, 3353, 3213,

2911, 2213, 1619, 1525, 1444, 1355, 1274, 1170, 948, 519; ^{1}H NMR (400 MHz, DMSO-d$_6$) δ (ppm): 7.19–7.37 (m, 2H, (Ar–H), 2H, NH$_2$), 6.81 (d, J = 8.0 HZ, 1H), 6.71 (s, 1H), 5.70 (s, 1H), 3.31–3.34 (m, 2H), 2.93 (s, 6H, 2CH$_3$), 2.09–2.21 (m, 2H), 1.45–1.68 (m, 3H), 0.79–0.85 (m, 1H).

3-Amino-1-(3-nitrophenyl)-5,6,7,8-tetrahydro-1H-isochromene-4-carbonitrile (4h). White solid; mp: 247–251 °C (Lit. mp 248–250 °C);[34] IR (KBr) $\bar{\nu}$ (cm^{-1}): 3440, 3356, 3249, 2948, 2209, 1638, 1530, 1441, 1351, 906, 828, 546; ^{1}H NMR (400 MHz, CDCl$_3$) δ (ppm): 7.47 (d, J = 8.0 Hz, 2H), 7.21–7.35 (m, 2H), 6.04 (s, 1H), 4.87 (s, 2H, NH$_2$), 3.03–3.06 (m, 1H), 2.83–2.88 (m, 1H), 2.27–2.32 (m, 1H), 2.15–2.19 (m, 1H), 1.79–1.81 (m, 1H), 1.69–1.73 (m, 1H), 1.53–1.60 (m, 1H), 0.90–1.00 (m, 1H).

3-Amino-1-(4-fluorophenyl)-5,6,7,8-tetrahydro-1H-isochromene-4-carbonitrile (4i). White solid; mp: 260–264 °C (Lit. mp 262–265 °C);[33] IR (KBr) $\bar{\nu}$ (cm^{-1}): 3417, 3340, 3245, 2947, 2211, 1646, 1603, 1510, 1391, 1231, 844, 572; ^{1}H NMR (400 MHz, DMSO-d$_6$) δ (ppm): 7.28–7.58 (m, 4H (Ar–H), 2H, NH$_2$), 5.73 (s, 1H), 3.62–3.65 (m, 1H), 2.80–2.83 (m, 1H), 2.06–2.22 (m, 2H), 1.66–1.69 (m, 1H), 1.44–1.47 (m, 2H), 0.80–0.90 (m, 1H).

3-Amino-1-(2-nitrophenyl)-5,6,7,8-tetrahydro-1H-isochromene-4-carbonitrile (4j). White solid; mp: 297–300 °C; IR (KBr) $\bar{\nu}$ (cm^{-1}): 3443, 3356, 2941, 2214, 1624, 1527, 1354, 1269, 727, 504; ^{1}H NMR (400 MHz, DMSO-d$_6$) δ (ppm): 8.09 (d, J = 8.0 Hz, 1H), 8.02 (d, J = 8.0 Hz, 1H), 7.93 (t, J = 8 Hz, 1H), 7.76 (t, J = 8.0 Hz, 1H), 7.44 (s, 2H, NH$_2$), 5.79 (s, 1H), 4.06–4.09 (m, 1H), 2.98–3.01 (m, 1H), 2.09–2.24 (m, 2H), 1.69–1.73 (m, 1H), 1.48–1.50 (m, 2H), 0.99–1.08 (m, 1H); ^{13}C NMR (100 MHz, DMSO-d$_6$) δ (ppm): 151.36, 143.60, 134.06, 131.11, 130.15, 128.58, 128.24, 125.92, 121.66, 112.46, 81.91, 45.38, 34.66, 27.06, 25.23, 21.26.

3-Amino-1-(2-bromophenyl)-5,6,7,8-tetrahydro-1H-isochromene-4-carbonitrile (4k). White solid; mp: 295–298 °C; IR (KBr) $\bar{\nu}$ (cm^{-1}): 3445, 3355, 2947, 2216, 1622, 1438, 1391, 1272, 1025, 746, 513; ^{1}H NMR (400 MHz, DMSO-d$_6$) δ (ppm): 7.78 (dd, J = 8.0 Hz, 2H), 7.58 (t, J = 8.0 Hz, 1H), 7.47 (s, 2H, NH$_2$) (exchange with D$_2$O), 7.41 (t, J = 8.0 Hz, 1H), 5.78 (s, 1H), 3.85–3.88 (m, 1H), 2.83–2.88 (m, 1H), 2.09–2.21 (m, 2H), 1.65–1.69 (m, 1H), 1.33–2.46 (m, 2H), 0.78–0.87 (m, 1H); ^{13}C NMR (100 MHz, DMSO-d$_6$) δ (ppm): 143.97, 134.04, 133.90, 131.44, 129.66, 128.99, 127, 121.38, 116.41, 112.70, 81.85, 49.73, 35.17, 27.23, 25.21, 21.26.

3-Amino-1-(4-methylphenyl)-5,6,7,8-tetrahydro-1H-isochromene-4-carbonitrile (4l). White solid; mp: 284–288 °C; IR (KBr) $\bar{\nu}$ (cm^{-1}): 3421, 3336, 2944, 2213, 1646, 1601, 1393, 1273, 1036, 829, 589; ^{1}H NMR (400 MHz, DMSO-d$_6$) δ (ppm): 7.46 (d, J = 8.0 Hz, 1H), 7.36 (s, 2H, NH$_2$), 7.30 (d, J = 8.0 Hz, 2H), 7.23 (s, 1H), 5.72 (s, 1H), 3.46–3.49 (m, 1H), 2.74–2.80 (m, 1H), 2.34 (s, 3H, CH$_3$), 2.06–2.21 (m, 2H), 1.67–1.69 (m, 1H), 1.43–1.50 (m, 2H), 0.80–0.89 (m, 1H); ^{13}C NMR (100 MHz, DMSO-d$_6$) δ (ppm): 144.07, 138.78, 132.73, 132.72, 132.05, 129.73, 129.39, 120.70, 116.65, 113.07, 81.96, 50.73, 34.35, 27.47, 25.33, 21.47, 21.21.

3. Results and discussion

3.1. Preparation and characterization of the catalyst

The Fe$_3$O$_4$@CS-SB-CaMgFe$_2$O$_4$ nanocatalyst was prepared according to Sections 2.2–2.5 and Fig. 1. The prepared nanocatalyst was characterized *via* FT-IR, XRD, VSM, FE-SEM, EDX, Mapp scanning, BET, and TGA techniques. The FT-IR spectra of the catalyst are shown in Fig. 2a–d. In the infrared spectrum in Fig. 2a, the peaks related to Mg–O and Fe–O bonds are observed in the region of 561 and 477 cm^{-1}, respectively. In Fig. 2b, it can be seen that the stretching vibration in the region of 3439 cm^{-1} is related to the O–H and N–H bonds of the chitosan compound and the stretching vibration in the region of 2868 cm^{-1} is related to the stretching C–H bond. The peak appearing in the region of 1408 cm^{-1} is related to the alcoholic OH of chitosan, and the stretching vibration in the region of 1080 cm^{-1} is related to the C–O bond. The peak in the region of 569 cm^{-1} is related to the stretching vibration of the Fe–O bond, which indicates the coating of Fe$_3$O$_4$ NPs with chitosan. In the infrared spectrum of Fe$_3$O$_4$@CS NPs in Fig. 2c, the peak appearing in the region of 2920 cm^{-1} is related to the C–H bond, and the peak in the region of 1558 cm^{-1} is related to the N–H bond of chitosan that binds the chitosan to the ferrite surface. Further, the band appearing at 1640 cm^{-1} is related to the stretching vibration of the azomethine group (CH=N). In the spectrum of Fig. 2d, it is shown that the peak of azomethine decreased to 1638 cm^{-1}, which indicates the coordination of CaMgFe$_2$O$_4$ nanoparticles with a nitrogen of azomethine.

The X-ray diffraction (XRD) patterns of CaMgFe$_2$O$_4$ NPs (a), Fe$_3$O$_4$@CS NPs (b), Fe$_3$O$_4$@CS-Schiff base (c), and Fe$_3$O$_4$@CS-SB-CaMgFe$_2$O$_4$ (d) are recorded and shown in Fig. 3. Fig. 3a is related to the X-ray diffraction of CaMgFe$_2$O$_4$ nanoparticle with crystal structure where 2θ is equal to 24.40, 33.44, 35.94, 41.13,

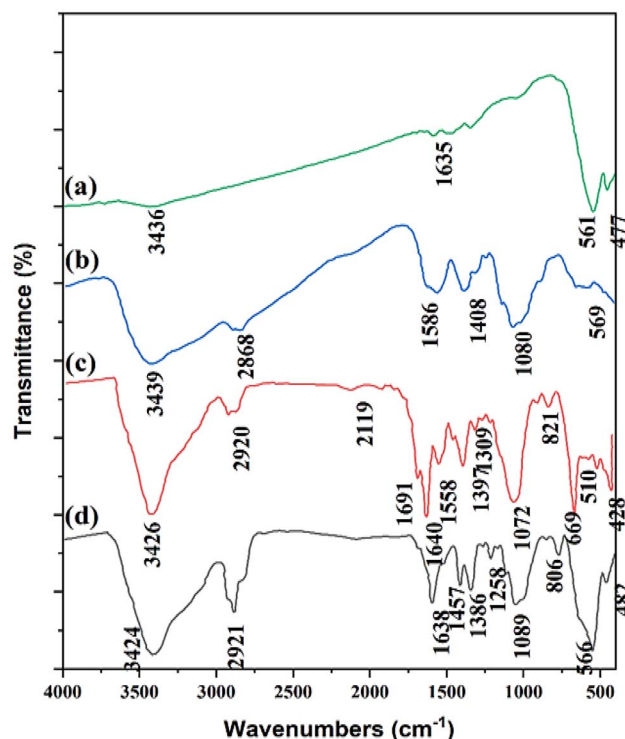**Fig. 2** FT-IR spectra of (a) CaMgFe$_2$O$_4$ NPs; (b) Fe$_3$O$_4$@CS NPs; (c) Fe$_3$O$_4$@CS-Schiff base; and (d) Fe$_3$O$_4$@CS-SB-CaMgFe$_2$O$_4$ nanocatalyst.

49.75, 54.33, 57.24, 57.24, 6627, 57.24, 6627 respectively. Fig. 3b corresponds to the fabrication of Fe_3O_4 coated with chitosan and shows a broad peak at $2\theta = 20.75$, 27.20, 35.62, 39.89, 46.96, 56.38, and 63.33. Fig. 3c is the diffraction pattern related to the structure of Fe_3O_4@CS NPs covered with terephthalaldehyde, which shows broad peaks at $2\theta = 20.81$, 27.16, 35.65, 39.71, 46.85, 56.39, 62.23, 64.55 and 68.29, respectively. Fig. 3d is related to the last stage of catalyst construction, which proves that the $CaMgFe_2O_4$ is well placed on Fe_3O_4@CS-Schiff base and 2θ is 24.32, 30.40, 33.34, 33.34, 41.04, 43.38, 49.63, 54.28, 57.56, 62.60, 64.15 and 75.25, respectively. Also, the diffraction pattern of Fe_3O_4@CS-SB-$CaMgFe_2O_4$ includes all characteristic peaks that match the standard XRD patterns. The size of the prepared nanoparticles was estimated to be 33 nm by the Debye–Scherrer equation.

By using VSM analysis, the magnetic properties of the $CaMgFe_2O_4$ NPs (Fig. 4a) and Fe_3O_4@CS-SB-$CaMgFe_2O_4$ nanocatalyst (Fig. 4b) were investigated. Fig. 4a is related to the $CaMgFe_2O_4$ nanoparticle with a magnetic property of 15.9 emu g^{-1}, and Fig. 4b is related to the last stage of the construction of this nanocatalyst whose magnetic property is equal to 8.25 emu g^{-1}. Due to the coating with Fe_3O_4@CS-Schiff base, the magnetic property of $CaMgFe_2O_4$ has decreased to 7.65 emu g^{-1}.

The size, morphology and uniformity of the fabricated nanocatalyst were investigated by FE-SEM analysis. As shown in Fig. 5, the spherical morphology of the Fe_3O_4@CS-SB-$CaMgFe_2O_4$ nanocatalyst can be well identified. The average size of these nanoparticles is 27.51 nm and they are three-dimensionally formed.
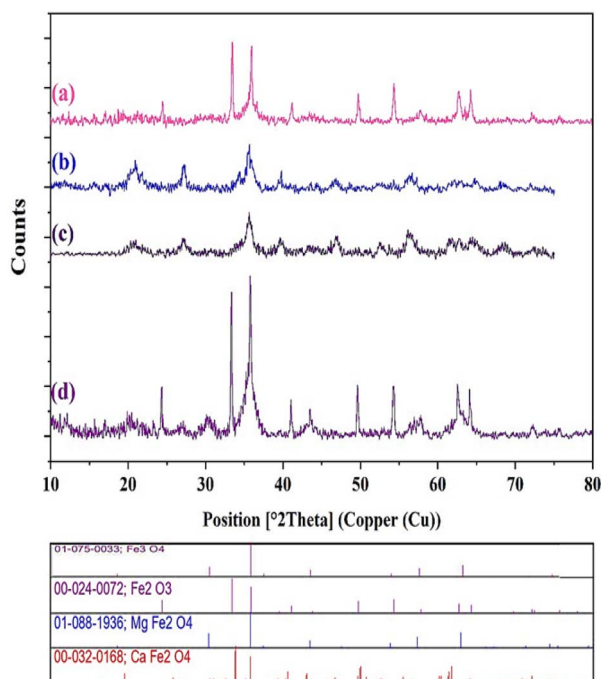
Furthermore, by using EDX analysis, presence of different elements on the surface of the Fe_3O_4@CS-SB-$CaMgFe_2O_4$ nanocatalyst was investigated. According to Fig. 6, the presence of peaks of iron, calcium, magnesium, and oxygen atoms confirms the existence of these elements in nanoparticles as a part of the nanocatalyst. Also, the percentage of these elements in the nanocatalyst is determined: oxygen 61.32%, carbon 30.14%, nitrogen 4.57%, magnesium 0.16%, calcium 0.58%, and iron 31.94%.

As can be seen in the images of mapping analysis (Fig. 7), the elements in the nanocatalyst are well distributed on the surface of this nanoparticle. By examining the dispersion of elements in this figure, it is proved that the oxygen, iron and carbon atoms have more dispersion than the calcium, magnesium and nitrogen.

The graph of thermal gravimetric analysis of the Fe_3O_4@CS-SB-$CaMgFe_2O_4$ catalyst is shown in Fig. 8. This nanoparticle is resistant to heat up to 800 °C. At a temperature of 100 °C, a slight weight loss is observed, which is related to the removal of water and solvents trapped in the catalyst. Also, the weight loss from 300 °C is related to the breaking of a part of the glycosidic bonds in the chitosan polymer stabilized on the surface of magnetic nanoparticles. The weight loss from the region of 600 to 800 °C is related to the chitosan chain and the destruction of the organic groups attached to the nanoparticles, which proves the placement of the organic groups on the nanoparticles.

The BET analysis of the Fe_3O_4@CS-SB-$CaMgFe_2O_4$ magnetic nanocatalyst is shown in Fig. 9. As can be seen in the BET diagram (a) the measured surface area of this sample is equal to 7.40 m^2 g^{-1}, the total volume of the measured holes ($P/P_0 = 0.982$) is equal to 0.075 cm^3 g^{-1} and the average size of the holes is equal to 40.82 nm. As can be seen in the adsorption and desorption diagram (b), this nanocatalyst is isotherm type (IV). Also, according to the BJH diagram (c), the abundance of holes is in the range of mesoporous (14.02 nm).
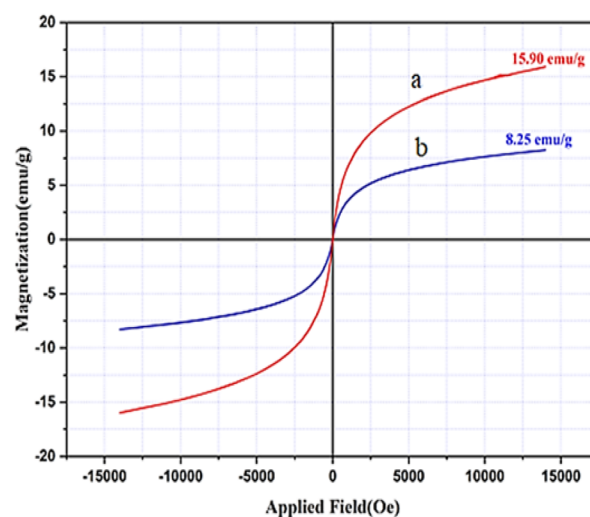

Fig. 3 XRD patterns of (a) $CaMgFe_2O_4$ NPs; (b) Fe_3O_4@CS NPs; (c) Fe_3O_4@CS-Schiff base; and (d) Fe_3O_4@CS-SB-$CaMgFe_2O_4$ nanocatalyst.

Fig. 4 The vibrating sample magnetometer curves of (a) $CaMgFe_2O_4$ NPs and (b) Fe_3O_4@CS-SB-$CaMgFe_2O_4$ nanocatalyst.
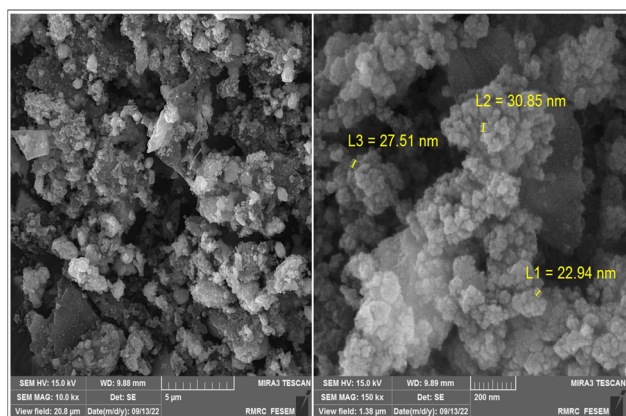
Fig. 5 FE-SEM images of the Fe_3O_4@CS-SB-CaMgFe$_2O_4$ nanocatalyst.
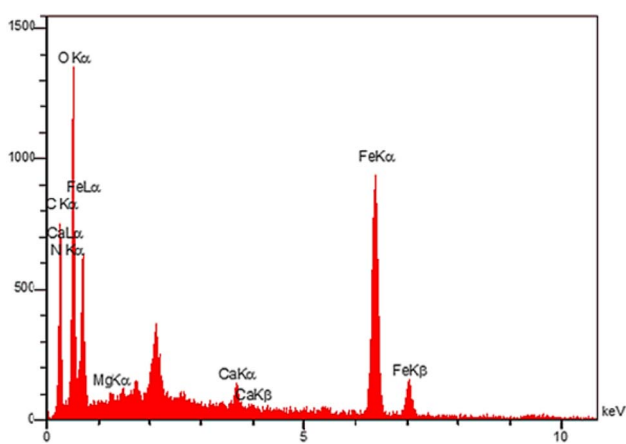
Fig. 6 EDX spectrum of the Fe_3O_4@CS-SB-CaMgFe$_2O_4$ nanocatalyst.

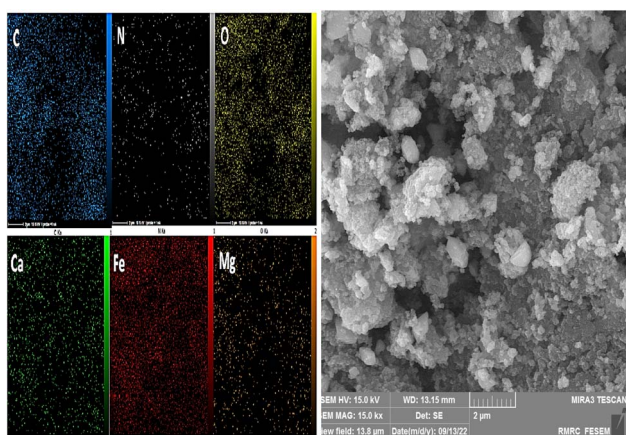**Fig. 7** Mapping images of the Fe_3O_4@CS-SB-CaMgFe$_2O_4$ nanocatalyst.

3.2. Investigation of catalytic activity in the reaction

The catalytic activity of Fe_3O_4@CS-SB-CaMgFe$_2O_4$ in the synthesis of 1H-isochromene compounds was investigated at

25 °C. In order to determine the most appropriate amount of the magnetic nanocatalyst, solvent, and temperature used in the reaction to obtain the highest efficiency, the cyclohexanone, malononitrile and benzaldehyde were reacted as a model reaction.

Initially, to achieve the most suitable catalyst amount in the synthesis of 1H-isochromenes, the reaction was investigated in the presence of different amounts of Fe_3O_4@CS-SB-CaMgFe$_2O_4$ magnetic nanocatalyst. The obtained results are given in Table 1.

As can be seen in this table, the best amount of nanocatalyst in this reaction in ethanol solvent and at room temperature is determined to be 10 mg with an efficiency of 97% at 10 minutes. By increasing the amount of optimized catalyst in the reaction, the yield and reaction time do not change.

To determine the most suitable solvent used in the reaction based on the highest product yield, the model reaction in the presence of 10 mg magnetic catalyst in various solvents such as $CHCl_3$, THF, DMF, CH_3OH, CH_3CN, H_2O/EtOH and EtOH solvents was performed at room temperature. The corresponding results are indicated in Table 2. As seen in Table 2, according to the results, the reaction in ethanol solvent gave the highest efficiency in the shortest time.

The three component reaction of 1 mmol of cyclohexanone, 1 mmol of malononitrile and 1 mmol of benzaldehyde in the presence of ethanol solvent and 10 mg of nanocatalyst has been investigated at different temperatures. The obtained results are shown in Table 3. As can be seen in this table, it was observed that the product yield increased with the decrease in temperature so that the reaction has the highest efficiency at room temperature.

To investigate the generality and development of this catalytic protocol, the reaction was carried out with various substituted aromatic aldehydes and using the fabricated nanocatalyst for the synthesis of 1H-isochromene derivatives under optimal conditions. The corresponding results are summarized in Table 4. According to the results of this table, aldehydes with electron-withdrawing groups have higher
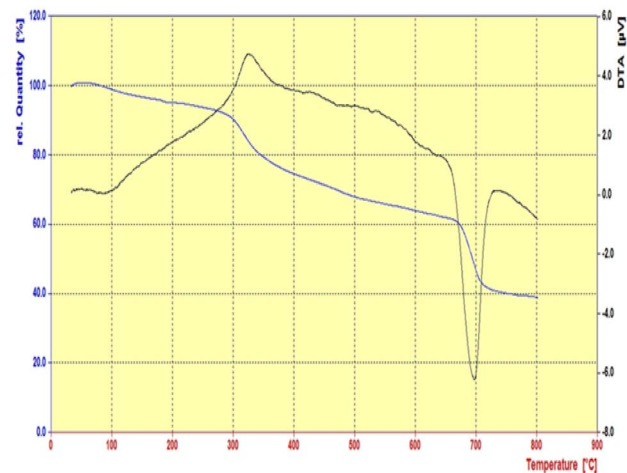

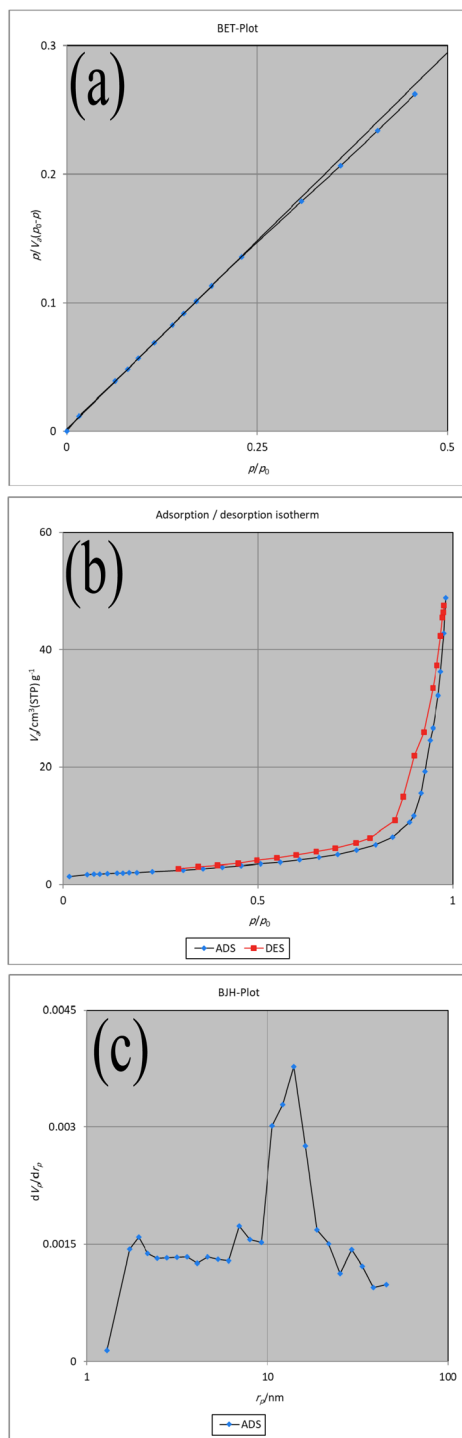**Fig. 8** TGA diagrams of the Fe_3O_4@CS-SB-CaMgFe$_2O_4$ nanocatalyst.

Fig. 9 (a) BET, (b) ADS/DES, and (c) BJH spectrum of the Fe$_3$O$_4$@CS-SB-CaMgFe$_2$O$_4$ nanocatalyst.

efficiency than the aldehydes with electron-donating groups in the reaction.

The comparison of catalytic activity of the presented nanocatalyst with the previously reported catalysts in the synthesis of 4d product is provided in Table 5. As shown in this table, the reaction for the preparation of this compound has a higher efficiency and a shorter duration in the presence of Fe$_3$O$_4$@CS-SB-CaMgFe$_2$O$_4$ nanocatalyst than the other catalysts.

Table 1 Optimization of Fe$_3$O$_4$@CS-SB-CaMgFe$_2$O$_4$ catalyst amount in the reaction^a

Entry	Catalyst (mg)	Time (min)	Yield^b (%)
1	—	80	10
2	6	40	60
3	8	20	86
4	10	10	97
5	12	10	97

^{a} Reaction conditions: benzaldehyde (1 mmol), malononitrile (1 mmol) and cyclohexanone (1 mmol), in the presence of different amounts of nanocatalyst, ethanol solvent (5 mL) and temperature (25 °C). ^{b} Isolated yield.

3.3. Proposed reaction mechanism for synthesis of 1H-isochromenes

The plausible reaction mechanism for the synthesis of 1H-isochromene derivatives is fully described in Scheme 1. According to this mechanism, the base nanocatalyst creates a negative charge by separating a hydrogen from malononitrile. Then, this negative charge causes a nucleophilic attack on the carbonyl group of cyclohexanone and forms the intermediate (1). The formed intermediate reacts with benzaldehyde to produce intermediate (2). Also, intermediate (3) is formed during a cyclization reaction of intermediate (2), and the target product is formed by the imine to enamine tautomerization of intermediate (3). Finally, the Fe$_3$O$_4$@CS-SB-CaMgFe$_2$O$_4$ catalyst is separated from the reaction medium for the next catalysis cycle.

3.4. Reusability

The possibility of reusing the catalyst is considered as an important feature from the economic, environmental, commercial, and industrial point of view. After the end of reaction, the Fe$_3$O$_4$@CS-SB-CaMgFe$_2$O$_4$ catalyst was separated from the reaction using an external magnet. Then, it was washed several times with chloroform and hot ethanol solvents and dried. As shown in Fig. 10, the recovered catalyst was used in five runs to prepare the 1H-isochromene compound and the efficiency and selectivity of the recovered catalyst remained substantially unaltered.

Table 2 Optimization of various solvents for the preparation of 1H-isochromenes^a

Entry	Solvent	Time (min)	Yield^b (%)
1	CHCl$_3$	70	20
2	THF	50	58
3	DMF	45	78
4	CH$_3$OH	30	80
5	CH$_3$CN	20	90
6	H$_2$O/EtOH	30	82
7	EtOH	10	97

^{a} Reaction conditions: benzaldehyde (1 mmol), malononitrile (1 mmol) and cyclohexanone (1 mmol), in the presence of 10 mg of nanocatalyst, different solvents and temperature (25 °C). ^{b} Isolated yield.
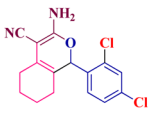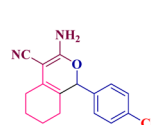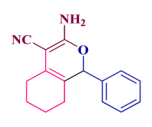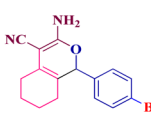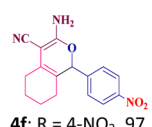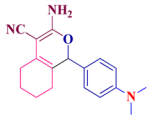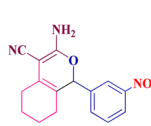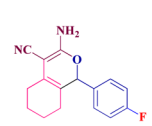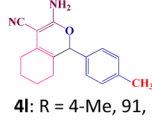
Table 3 Optimization of temperatures for the preparation of 1*H*-isochromene derivatives[a]

Entry	Temperature	Time (min)	Yield[b] (%)
1	70	80	70
2	60	50	74
3	50	35	87
4	40	20	91
5	25	10	97

[a] Reaction conditions: benzaldehyde (1 mmol), malononitrile (1 mmol) and cyclohexanone (1 mmol), in the presence of 10 mg of nanocatalyst, 5 mL of ethanol solvent, at different temperatures. [b] Isolated yield.

Table 4 Synthesis of 1*H*-isochromene derivatives at room temperature[a]

4a-l	Yield[b] (%)	Time (min)

4a: R = 2,4-dichloro, 95, 13

4b: R = 4-Cl, 93, 20

4c: R = 2-Cl, 96, 12

4d: R = H, 97, 10

4e: R = 4-Br, 97, 10

4f: R = 4-NO$_2$, 97, 10

4g: R = N, *N*-dimethyl, 91, 25

4h: R = 3-NO$_2$, 93, 20

4i: R = 4-F, 92, 22

4j: R = 2-NO$_2$, 97, 10

4k: R = 2-Br, 97, 10

4l: R = 4-Me, 91, 25

[a] Reaction conditions: aldehyde derivatives (1 mmol), malono-nitrile (1 mmol) and cyclohexanone (1 mmol), in the presence of 0.01 g of nanocatalyst, 5 mL of ethanol solvent, at 25 °C. [b] Isolated yield.

Table 5 Comparison of the catalytic activity of the Fe$_3$O$_4$@CS-S.B-CaMgFe$_2$O$_4$ nanocatalyst with the other reported catalysts for synthesis of 1*H*-isochromene derivatives

Entry	Compound	Time (min)	Yield[e] (%)	Ref.
1[a]	**4a**	20	90	34
2		13	95	This work
3[b]		30	92	33
4[c]	**4d**	240 (4 h)	55	35
5		10	97	This work
6[d]	**4e**	17	95	32
7		10	97	This work

[a] Morpholine (0.1 mmol, ethanol, 25 °C). [b] Nano CaMgFe$_2$O$_4$ (0.1 mmol, ethanol, 25 °C). [c] AcONa (2 g, ethanol, reflux). [d] Hollow MgO/SiO$_2$ nanocomposites (10 mg, ethanol, 25 °C). [e] Isolated yield.

Fig. 11a presents the field emission scanning electron microscopy (FE-SEM) image of the recovered catalyst. It can be observed that the morphology of the catalyst remains unchanged after recovery. Moreover, Fig. 11b illustrates the X-ray diffraction (XRD) pattern of the recovered catalyst, which exhibits no discernible variations when compared to the XRD pattern of the catalyst prior to its use as a catalyst. Upon analyzing the recovered catalyst, it was determined that the catalyst exhibited remarkable stability within the reaction environment and did not experience any deterioration in its catalytic performance. The FT-IR spectrum of the Fe$_3$O$_4$@CS-SB-CaMgFe$_2$O$_4$ nanocatalyst after recovery is presented in Fig. 11c. By analyzing and examining the FT-IR spectrum after the recovery of the nanocatalyst, we concluded that no new peaks were added compared to the nanocatalyst before recovery and the previous peaks were
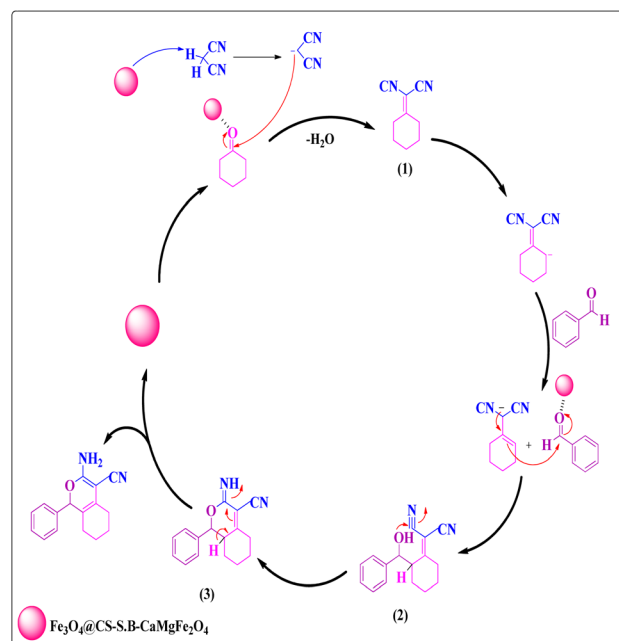
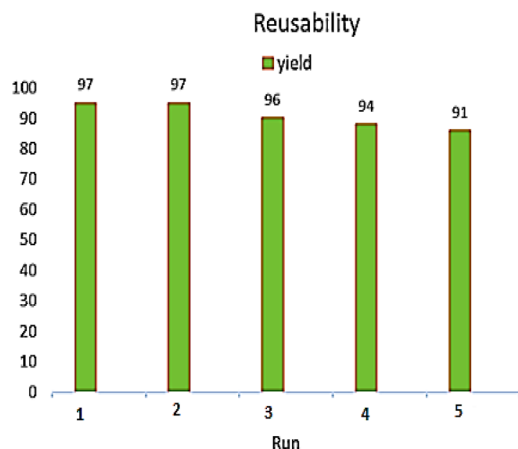**Scheme 1** Proposed reaction mechanism for the synthesis of 1*H*-isochromenes.

observed, which shows that the functional groups in the Fe$_3$O$_4$@CS-SB-CaMgFe$_2$O$_4$ nanocatalyst structure remained intact after recovery.
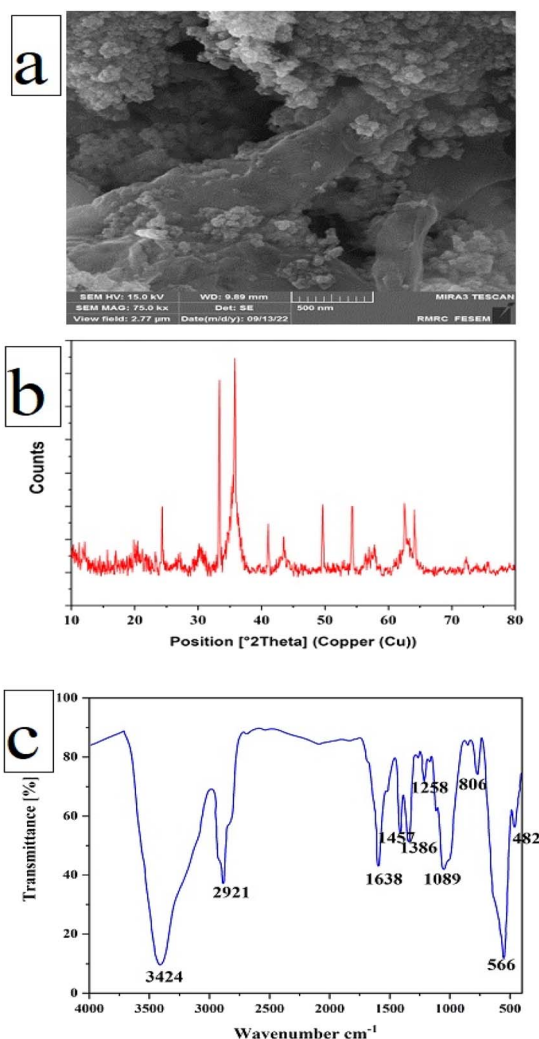
The leaching test of the Fe$_3$O$_4$@CS-SB-CaMgFe$_2$O$_4$ nanocatalyst was performed using the hot filtration method. The reaction of cyclohexanone, malononitrile, and benzaldehyde in the presence of Fe$_3$O$_4$@CS-SB-CaMgFe$_2$O$_4$ nanocatalyst was stopped after 5 minutes and then the nanocatalyst was separated from the reaction mixture using an external magnet. Next, the filtrate mixture was stirred and the progress of the reaction was monitored with thin layer chromatography (TLC) techniques. The monitored reaction did not progress after filtration, so the hot filtration analysis shows that leaching the Fe$_3$O$_4$@CS-SB-CaMgFe$_2$O$_4$ nanocatalyst does not happen.

4. Conclusions

The aim of this research was to identify, prepare, and develop a high-efficiency and environmentally friendly nanocatalyst. To increase the chemical stability and biocompatibility of iron oxide nanoparticles, these nanoparticles were coated with chitosan. Polymer-coated superparamagnetic nanoparticles are usually in the form of a magnetic core and a polymer shell with desired functional groups. These nanoparticles have features such as easy separation using an external magnetic field and the ability to extract a large volume of the sample. When the magnetic nanoparticles are coated, these nanoparticles are not destroyed in the reaction conditions, and it is possible to recover and reuse the catalyst, which makes the recovery of the catalyst economical and saves the environment. In addition, increasing the surface increases the activity of the catalyst as well as increasing the reaction efficiency and reducing the reaction time. The Fe$_3$O$_4$@CS-SB-CaMgFe$_2$O$_4$ nanocatalyst was used as a green and recyclable magnetic nanocatalyst for the synthesis of 1*H*-isochromene derivatives at room temperature. The advantages of this method include a wide range of products, excellent reaction efficiency, and the ability to recycle and reuse the catalyst.

Conflicts of interest

There are no conflicts to declare.

Acknowledgements

References

1 E. Khan, M. Hanif and M. S. Akhtar, *Rev. Inorg. Chem.*, 2022, **42**, 307–325.
2 E. Raczuk, B. Dmochowska, J. Samaszko-Fiertek and J. Madaj, *Molecules*, 2022, **27**, 787.
3 H. Schiff, *Ann. Chem. Pharm.*, 1864, **131**, 118–119.
4 H. Naeimi, F. Salimi and K. Rabiei, *J. Mol. Catal. A: Chem.*, 2006, **260**, 100–104.
5 M. Gupta, S. Sihag, A. K. Varshney and S. Varshney, *J. Chem.*, 2013, **2013**, 1–8.

6   A. Hameed, M. Al-Rashida, M. Uroos, S. Abid Ali and K. M. Khan, *Expert Opin. Ther. Pat.*, 2017, **27**, 63–79.

7   J. Ceramella, D. Iacopetta, A. Catalano, F. Cirillo, R. Lappano and M. S. Sinicropi, *Antibiotics*, 2022, **11**, 191.

8   D. Iacopetta, R. Lappano, A. Mariconda, J. Ceramella, M. S. Sinicropi, C. Saturnino, M. Talia, F. Cirillo, F. Martinelli, F. Puoci, C. Rosano, P. Longo and M. Maggiolini, *Int. J. Mol. Sci.*, 2020, **21**, 7797.

9   A. Catalano, M. S. Sinicropi, D. Iacopetta, J. Ceramella, A. Mariconda, C. Rosano, E. Scali, C. Saturnino and P. Longo, *Appl. Sci.*, 2021, **11**, 6027.

10 K. S. Munawar, S. M. Haroon, S. A. Hussain and H. Raza, *J. Basic Appl. Sci.*, 2018, **14**, 217–229.

11 S. Liu, B. Yu, S. Wang, Y. Shen and H. Cong, *Adv. Colloid Interface Sci.*, 2020, **281**, 102165.

12 X. Batlle, C. Moya, M. Escoda-Torroella, Ò. Iglesias, A. Fraile Rodríguez and A. Labarta, *J. Magn. Magn. Mater.*, 2022, **543**, 168594.

13 T. C. Braga, M. M. Silva, E. O. O. Nascimento, E. C. Dantas da Silva, Y. de Freitas Rego, M. Mandal, Z. Alves de Souza, A. L. Tasca Góis Ruiz, J. Ernesto de Carvalho, F. T. Martins, I. M. Figueiredo, T. Mendonça de Aquino, C. Moreira da Silva, B. Mandal, G. Brahmachari, J. C. Caldas Santos and Â. de Fátima, *Eur. J. Med. Chem. Rep.*, 2022, **4**, 100030.

14 G. R. Rodrigues, C. López-Abarrategui, I. de la Serna Gómez, S. C. Dias, A. J. Otero-González and O. L. Franco, *Int. J. Pharm.*, 2019, **555**, 356–367.

15 C. P. Jiménez-Gómez and J. A. Cecilia, *Molecules*, 2020, **25**, 3981.

16 C.-L. Ke, F.-S. Deng, C.-Y. Chuang and C.-H. Lin, *Polymers*, 2021, **13**, 904.

17 S. Kim, *Int. J. Polym. Sci.*, 2018, **2018**, 1–13.

18 G. Benchamas, G. Huang, S. Huang and H. Huang, *Trends Food Sci. Technol.*, 2021, **107**, 38–44.

19 W. Zhao, M. Adeel, P. Zhang, P. Zhou, L. Huang, Y. Zhao, M. A. Ahmad, N. Shakoor, B. Lou, Y. Jiang, I. Lynch and Y. Rui, *Environ. Sci.: Nano*, 2022, **9**, 61–80.

20 S. Lahouti and H. Naeimi, *RSC Adv.*, 2020, **10**, 33334–33343.

21 T. Huq, A. Khan, D. Brown, N. Dhayagude, Z. He and Y. Ni, *J. Bioresour. Bioprod.*, 2022, **7**, 85–98.

22 J. C. M. Souza, V. Fernandes, A. Correia, P. Miller, O. Carvalho, F. Silva, M. Özcan and B. Henriques, *Clin. Oral Invest.*, 2022, **26**, 95–107.

23 M. Kołodziejska, K. Jankowska, M. Klak and M. Wszoła, *Nanomaterials*, 2021, **11**, 3019.

24 H. Naeimi and S. Lahouti, *Appl. Organomet. Chem.*, 2017, **31**, e3732.

25 Y.-C. Chang and D.-H. Chen, *J. Colloid Interface Sci.*, 2005, **283**, 446–451.

26 D. L. Poeira, J. Macara and M. M. B. Marques, in *Comprehensive Heterocyclic Chemistry IV*, Elsevier, 2022, pp. 243–328.

27 Z. Zhao, K. Kang, J. Yue, X. Ji, H. Qiao, P. Fan and X. Zheng, *Eur. J. Med. Chem.*, 2021, **210**, 113073.

28 V. V. Dabholkar and D. R. Tripathi, *J. Heterocycl. Chem.*, 2011, **48**, 529–532.

29 M. M. Khafagy, A. H. Abd El-Wahab, F. A. Eid and A. M. El-Agrody, *Farm*, 2002, **57**, 715–722.

30 N. Nardangeli, J. Thomson, N. Topolovčan and T. Hudlický, *Synthesis*, 2021, **53**, 4110–4116.

31 H. Zhan, M. Hou, Y. Li, Z. Chen, Y. Wei and S. Liu, *ChemistrySelect*, 2021, **6**, 11537–11540.

32 S. Mohammadi and H. Naeimi, *Silicon*, 2022, **14**, 6881–6893.

33 H. Naeimi and S. Mohammadi, *J. Heterocycl. Chem.*, 2020, **57**, 50–59.

34 H. Naeimi and S. Mohammadi, *ChemistrySelect*, 2020, **5**, 2627–2633.

35 A. M. El-Sayed and H. Abdel-Ghany, *J. Heterocycl. Chem.*, 2000, **37**, 1233–1240.